Materials Today Bio 27 (2024) 101160

Contents lists available at ScienceDirect

Materials Today Bio

journal homepage: www.journals.elsevier.com/materials-today-bio

Omnidirectional anisotropic embedded 3D bioprinting

Lei Shao [a,b,c,*], Jinhong Jiang [a,c], Chenhui Yuan [a,d], Xinyu Zhang [a,c], Lin Gu [a,c], Xueping Wang [a,b,**]

[a] Research Institute for Medical and Biological Engineering, Ningbo University, Ningbo, 315211, Zhejiang, China
[b] State Key Laboratory of Fluid Power and Mechatronic Systems, College of Mechanical Engineering, Zhejiang University, Hangzhou, 310027, Zhejiang, China
[c] Health Science Center, Ningbo University, Ningbo, 315211, Zhejiang, China
[d] School of Materials Science & Chemical Engineering, Ningbo University, Ningbo, 315211, China

ARTICLE INFO

Keywords:
Shear-oriented bioink
Embedded 3D bioprinting
Anisotropy
Muscle patch

ABSTRACT

Anisotropic microstructures resulting from a well-ordered arrangement of filamentous extracellular matrix (ECM) components or cells can be found throughout the human body, including skeletal muscle, corneal stroma, and meniscus, which play a crucial role in carrying out specialized physiological functions. At present, due to the isotropic characteristics of conventional hydrogels, the construction of freeform cell-laden anisotropic structures with high-bioactive hydrogels is still a great challenge. Here, we proposed a method for direct embedded 3D cell-printing of freeform anisotropic structure with shear-oriented bioink (GelMA/PEO). This study focuses on the establishment of an anisotropic embedded 3D bioprinting system, which effectively utilizes the shear stress generated during the extrusion process to create cells encapsulating tissues with distinct anisotropy. In conjunction with the water-solubility of PEO and the in-situ encapsulation effect provided by the carrageenan support bath, high-precise cell-laden bioprinting of intricate anisotropic and porous bionic artificial tissues can be effectively implemented in one-step. Additionally, anisotropic permeable blood vessel has been taken as a representation to validate the effectiveness of the shear-oriented bioink system in fabricating intricate structures with distinct directional characteristics. Lastly, the successful preparation of muscle patches with anisotropic properties and their guiding role for cell cytoskeleton extension have provided a significant research foundation for the application of the anisotropic embedded 3D bioprinting system in the ex-vivo production and in-vivo application of anisotropic artificial tissues.

1. Introduction

In the human body, nature has designed many tissues with anisotropic structures that result from the aligned arrangement of extracellular matrix (ECM) components or cells [1–3]. The intricate anisotropic topography and hierarchical structure of native ECMs not only impart highly-anisotropic mechanical properties to tissues but also govern cell response, encompassing spreading, migration, and morphology [4,5]. These distinct characteristics exhibit a strong dependence on the specific tissue involved. The bioinspired design is widely applied in tissue engineering to fabricate anisotropic structures possessing specific functionalities, such as cytoskeleton shape transformation and polarized patterning [6–8].

Among all the advanced approaches applied to fabricate anisotropic structures, such as micropatterning [9,10], electrospinning [11,12], and self-assembly [13,14], 3D bioprinting have received more attention for the practical application and controllable fabrication processes. Hydrogels are a type of the most crucial component of bioinks used in 3D bioprinting that bears resemblance to biological tissues and organs in many aspects, while most of them exhibits the inherent isotropic characteristics [15,16]. Considering these aspects, it is undeniable that developing anisotropic hydrogels provides an excellent entry point for the fabrication of 3D complex structures with anisotropic properties by 3D bioprinting. In order to fabricate anisotropic hydrogel that emulate the hierarchical organization observed in natural tissues and exhibit distinctive functionalities, numerous researchers recently have explored diverse approaches to induce alignment at no matter the microscopic level of molecular chains or the macroscopic level of structural orientation, such as mechanical forces [17], magnetic [15], electric fields [18] and gradients of temperature and ions [19,20]. However, these

* Corresponding author. Research Institute for Medical and Biological Engineering, Ningbo University, Ningbo 315211, Zhejiang, China.
** Corresponding author. Research Institute for Medical and Biological Engineering, Ningbo University, Ningbo 315211, Zhejiang, China.
E-mail addresses: shaolei1@nbu.edu.cn (L. Shao), wangxueping@nbu.edu.cn (X. Wang).

https://doi.org/10.1016/j.mtbio.2024.101160
Received 23 May 2024; Received in revised form 8 July 2024; Accepted 16 July 2024
Available online 17 July 2024

methods prepared anisotropic hydrogel materials relay on the real-time cross-linking to maintain the directional microstructures within the hydrogel fibers, impeding their application in anisotropic complex biomimetic tissue structure carriers.

Additionally, in present-day, to prepare anisotropic biomimetic artificial tissues with 3D bioprinting, it's crucial to combine hydrogels that possess both high bioactivity and customizable formability [20,21]. GelMA, the methacrylated gelatin, is currently receiving increased attention due to its superior bio-functionality [22]. When GelMA is employed in 3D bioprinting of anisotropic artificial tissues in millimeter-level, in addition to transforming its inherent isotropic properties, the naturally compact micropore structure should also be modified by enhancing the pore size to optimize transport efficiency and meet cell growth requirements. Furthermore, the mechanical strength of high biocompatible hydrogels is generally inadequate and the printability is undesirable, rendering them unsuitable for direct 3D bioprinting [23,24]. Consequently, high bioactive anisotropic hydrogels that can be used in 3D bioprinting need to be further developed.

In summary, there are three challenges in the preparation of high biocompatible anisotropic tissue structures with 3D bioprinting technology: 1) manipulating the orientation of hydrogel molecular chains to obtain anisotropic hydrogel mediated structures; 2) elevating the porosity of hydrogels to strengthen the mass transfer efficiency of the encapsulated cells; and 3) enhancing the printability of low-viscosity hydrogels. According to the kinetics of phase separation, multi-materials formed single/multiple continuous phases can be utilized for the preparation of porous structures [25,26]. By applying directional force, oriented anisotropic structures can be fabricated along with the mechanism of phase separation. Once a type of multiphase material solidifies, with the water-soluble characteristics of other phases, these can be efficiently dissolved during the cultivation process, enabling the effective preparation of porous oriented structures.

In this study, a shear-oriented bioink was prepared by combining polyethylene oxide (PEO), a typical thickening spinning agent, with low-viscosity and high biocompatibility GelMA. During the extrusion printing process, GelMA/PEO mixtures experiences shear forces provided by the inner wall of the needle that result in shear orientation characteristics. After printing, GelMA/PEO is solidified through light cross-linking. Utilizing the principle of multiphase separation and PEO's water-soluble nature, PEO can be effectively dissolved to prepare GelMA fibers with oriented microstructure and porosity. The embedded 3D bioprinting is a pioneering technology that provides temporary support for bioinks with limited mechanical strength or low viscosity, enables the preservation of assembled structure and prevents any potential collapse due to gravitational forces [27,28]. In combination with the κ-carrageenan (Car) support bath developed in our laboratory, the oriented fibers extruded from shear-oriented bioink can be instantly encapsulated by Car granular. This process not only preserves the internal, directionally-specific microscopic structure of the fibers, but it also allows for the possibility of their freeform assembly (Fig. 1). With this anisotropic embedded 3D bioprinting system, the shear-oriented bioink encapsulated different cell can be embedded 3D printed into any oriented complex tissue, providing a novel preparation strategy for the in-vitro construction of anisotropic bionic artificial tissues.

2. Method and materials

2.1. Materials

Gelatin (9000-70-8, Sigma-Aldrich, USA) methacrylate anhydride, methacrylate, dialysis bags (8000-14000D, D0405, Sigma-Aldrich, USA), rhodamine B and calcein labeled GelMA (EFL-GM-RF-60, EFL-GM-GF-60, Engineering For Life, China), phosphate buffered saline (PBS), 0.22 μm filter (Millipore), DMEM (high glucose, 11995-065, Thermo Fisher Scientific, USA), MEM-α (12571063, Thermo Fisher Scientific, USA) and penicillin-streptomycin (15140-122, Thermo Fisher

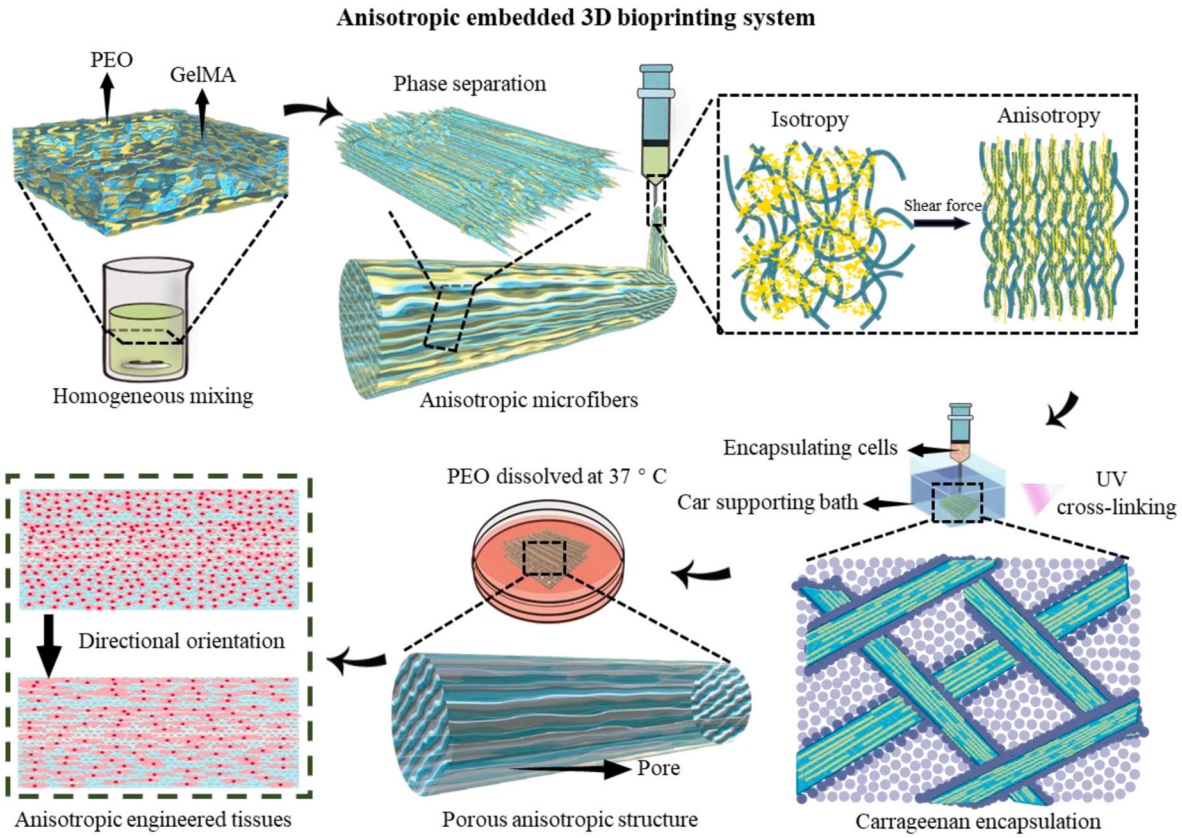

Fig. 1. The schematic diagram of the anisotropic embedded 3D bioprinting system.

Scientific, USA) were purchased from Hangjing (Hangjing Biological Technology Co., Ltd, Ningbo, China). Lithium phenyl-2, 4, 6 - trimethylbenzoylphosphonate (LAP, 900889, Sigma-Aldrich, USA) and Carrageenan were purchased from Sigma (C1138, Sigma-Aldrich, USA). The intensity of the blue light source at the crosslinking plane was 100 mw/cm2 to completely photocrosslink the GelMA.

The GelMA was synthesized as the same procedure reported [3]. Briefly, (1) 100 mL 10 % (w/v) gelatin solution prepared with PBS at 50 °C. (2) Added 2 mL methacrylate anhydride (MA, 276685, Sigma-Aldrich, USA) slowly to step (1) solution, synthesis reaction under stirring at 50 °C for 3 h (3) Added 400 ml PBS to step 2 reaction liquid, terminated reaction by stirring and diluting. (4) Solution from step (3) loaded into dialysis bags (8000-14000D), dialyzed continuously at 37 °C until TDS <5 through changing deionized water. (5) Dialysis solution pre-frozen at low temp (−20 °C or −80 °C) for 2 h, then freeze-dried for later use.

2.2. Preparation of bioink

Prior to bioprinting, the PEO with different molecular weight (100w, 200w, 400w and 710w) was irradiated by ultraviolet light for more than 30 min and added into 5 % GelMA solution (containing 0.25 % LAP, and filtered by 0.22um filter membrane) to the 1.5 % w/v concentration. The mixed solution was stirred at 37 °C for 3 h to completely dissolve, and transferred to 10 ml syringes, turned into PEO/GelMA bioink by cooling (25 °C for 10 min). The optimal molecular weight of PEO was added into 5 % GelMA solution at different concentration (0.5 % w/v, 1 % w/v, 1.5 w/v and 2 % w/v). The PEO/GelMA solution was mixed with corresponding cells for the bioprinting of cell-laden buildings. It is important to note that, in the process of bioprinting, the room temperature should be stayed at 25 °C and the syringe should be turned over at regular intervals (20 min) for uniform mixing of cells.

2.3. Preparation of κ-carrageenan suspensions

The κ-carrageenan (sigma) was added to 100 mL of Phosphate buffer solution (PBS, Solarbio), heated and stirred at 70 °C for 30 min to obtain a 0.7 w/v κ-carrageenan solution. The prepared solution was then autoclaved at 121 °C for 20 min. After that, the sterile κ-carrageenan solution was refrigerated for at least 2 h until complete gelation occurred. The resulting gel was crushed into particles with electric blender running at a speed of 1000 rpm/min. Subsequently, the support bath consisting of κ-carrageenan microgel particles was packed into 50 mL Nest centrifuge tube and centrifuged at a speed of 1000 rpm/min to remove any bubbles present. If not used immediately, the unused κ-carrageenan support bath can be stored in the refrigerator (4 °C) for up to one month or more but should be brought back to room temperature before use.

2.4. Physiochemical characterization of hydrogels

The rheological behaviors of PEO/GelMA hydrogel with different PEO concentration were monitored with a Discovery Hybrid Rheometer (TA Instruments, HR 30). Each measurement was carried out by a fresh sample loaded between the parallel plates with a gap value of 100 μm and removal of excessive sample. The storage modulus (G′), loss modulus (G′′) and gel point (sol-gel transition point) were determined by time-sweep mode at a constant oscillator frequency (10 rad/s) and strain (10–10^3 %) using a 40 mm diameter parallel plate geometry at 25 °C. At a given shear rate parameter, ranging from 10^{-3} to 100 s^{-1} with 25 measuring points, the relationship of viscosity and shear stress as a function of shear rate was recorded. The viscoelastic behavior was also analyzed by creep and creep-recovery experiments by applying two shear stress steps, the constant stress (10^{-6} MPa) at creep interval (0–180 s) followed by creep-recovery interval (180–350 s) after the removal of applied stress at 25 °C. The values of viscosity (η*) were recorded at Flow peak hold model, and the shear rate went down from 50 to 0.1 s^{-1}, and back to 50 s^{-1}. Phase-transition of viscosity was determined from the inflection points of the recorded graphs.

The degradation experiment involved placing gel blocks formed from 5 % GelMA containing 1 % PEO (400w molecular weight) in sterile PBS, maintaining a temperature of 37 °C for 14 days. At regular intervals, samples were collected, washed with deionized water, freeze-dried, and weighed. The remaining sample mass was then divided by the original sample mass to calculate the gel's degradation efficiency.

The hydrogels were frozen in liquid nitrogen and then dried by a freeze drier (Beijing Bo Medical Laboratory Instrument Co., Ltd.), observed by a scanning electron microscope (SEM, Hitachi, SU5000) at 15 kV accelerating voltage condition and analyzed the porosity with ImageJ software.

The fluorescence labeled GelMA was mixed with PEO and printed into different anisotropic structures which were imaged under a confocal fluorescence microscope (Olympus FV3000 microscopy).

2.5. Bioprinting process

The G-code for the raster structure was obtained by looping through Python (https://www.python.org/), which was developed by our laboratory. Self-assembling mechanical 3D extruder printers were used for printing. All models were sliced into STL format using Repetier-Host (https://www.repetier.com/). The printing process was conducted at room temperature. The dispensing needle and the 5 mL syringe were used for printing, ensuring a stable connection between the needle and syringe, preventing any loosening of the needle during printing. A petri dish with a diameter of 2 cm or a clear container measuring 2.5 cm × 3 cm × 3 cm was utilized to support the bath. The printed structures were exposed to a 3 w 405 nm UV light source (UltrFire) for 17 s, and removed directly with a spoon and placed in a beaker containing PBS, where it was heated at 37 °C until the suspension around the model dissolved.

For cell-loaded printing, the printer, ultra-clean table, and operating room were irradiated for at least 30 min before use. All glass and metal instruments related to printing were steam sterilized (121 °C, 20 min). The printed structures were exposed to 405 nm UV light source (UltrFire) for 17 s, then removed with a spoon and placed in the medium. After incubation in a constant temperature incubator at 37 °C for 30 min, the structures were appropriately washed with PBS to ensure removal of the support bath, lastly, the fresh medium was added.

2.6. Cell culture

MC3T3-E1 fibroblast cell line and structures containing 3T3 were cultured in α-MEM supplemented with 10 % FBS (16000-044, Thermo Fisher Scientific, USA) and 0.1 % w/v penicillin-streptomycin solution. BMSCs and HUVECs and cell loaded structures were cultured in DMEM supplemented with 10 % FBS and 0.1 % w/v penicillin-streptomycin solution. C2C12 and bioprinted structures were cultured in DMEM/F 12 supplemented with 10 % FBS and 0.1 % w/v penicillin-streptomycin solution. All cells were obtained from iCell Bioscience Inc, Shanghai. The structures were cultured in a CO_2 incubator (IL-161CT, STIK, China) at 37 °C. Printed structures were placed in new culture dishes and fresh medium was added every two days after removal of the support material.

2.7. Biological characterization of cell-laden scaffolds

The cell morphologies were characterized by staining F-actin and nuclei. The F-Actin and nuclei were stained with TRITC phalloidin and DAPI, respectively. The detailed process is as follows: (1) The cell-laden structures were washed with PBS and fixed in 4 % paraformaldehyde for 30 min (2) The cell-laden scaffolds were then washed with PBS and permeabilized with 0.5 % Triton X-100 for 5 min (3) Cell-laden structures were washed with PBS and stained with TRITC phalloidin (diluted

with 1 %(w/v) bovine serum albumin solution as instructed) for 30 min in the dark. (4) The cell-laden structures were washed in PBS again and stained with DAPI (10 μg/mL) for 10 min (5) Finally, the cell-laden structures were washed with PBS and imaged under a confocal fluorescence microscope (Leica TCS SP8, Wetzlar, Germany).

The culture medium was removed and replaced with cold PBS. Then the structures were washed 3 times with PBST and incubated with 4 % paraformaldehyde for 30 min on ice. After being washed 3 times, the structures were incubated with PBSDT blocking solution (PBS supplemented with 0.3 % Triton X-100, 1 % DMSO, 3 % BSA, and 1 % goat serum) for 2 h at room temperature, and incubated with one of the following primary antibodies: mouse anti-Myosin (1:250, Abcam, Cambridge, UK) and rabbit anti-Myogenin (1:250, Abcam, Cambridge, UK) for 12 h with gentle agitation at 4 °C. Subsequently, the structures were washed 3 times with PBST and incubated with Alexa Fluor 488-conjugated goat anti-rabbit antibody (1:250, Abcam, Cambridge, UK) and Alexa Fluor 594-conjugated goat anti-mouse antibody (1:250, Abcam, Cambridge, UK) for 2 h at room temperature with gentle agitation and then washed 3 times with PBST. Finally, the structures were stained with 4′,6diamidino-2-phenylindole (1:2000, Sigma Aldrich, St. Louis, MO, USA) for 15 min, and observed under a confocal microscope (Leica TCS SP8, Wetzlar, Germany).

2.8. Statistical analysis

Data were expressed as means ± SD deviation. All the histogram results were statistically analyzed by the GraphPad Prism Version 5.0 software. The polar coordinate statistical diagram was analyzed by the origin Version 2021 software. And the thickness of filaments and statistics of cell spreading was measured by the ImageJ.

3. Results and discussion

3.1. Composition optimization and printability confirmation of shear-oriented bioink

It has been reported that GelMA and PEO could be uniformly mixed but would gradually separate after long-time standing [3]. The mixture of GelMA and PEO with varying molecular weights was extruded into the supporting bath of Car. The fibers exhibited directional orientation characteristics to varying degrees. As shown in Fig. S1, due to the absence of a precross-linking environment in the Car bath, the retention time of the anisotropic microstructures of the GelMA/PEO fiber was limited, which is significantly exacerbated with low molecular weight PEO. Even though the molecular weight of PEO was 400 w or 710 w, the oriented fibers extruded by the GelMA/PEO mixture maintained their anisotropic characteristics in a Car bath for 30 min. The phase separation phenomena of GelMA and PEO under static conditions contribute to this result. The high molecular weight PEO increases the viscosity of the GelMA/PEO mixture, reducing the flow rate and extending stabilization time. To maximize the stability duration of the oriented structure, simultaneously reduce the viscosity of the material for its application during the printing process and the effective dissolution of PEO, the PEO with a molecular weight of 400w was chosen in subsequent experiments of this study.

To investigate the impact of varying concentrations of PEO on the printability of GelMA/PEO bioink, rheological experiments were conducted to simulate ink force, and a mechanical analysis was performed to assess the effect of different PEO concentrations on the ink system. The critical strain of GelMA is observed to be the highest in Fig. 2Aa, while an increase in PEO concentration gradually reduces the critical strain of the mixture. Homogeneous soft materials typically exhibit relatively high critical strains, and a higher volume fraction of the dispersed phase within the heterogeneous phase results in a smaller critical strain [29]. In order to investigate the stress reduction before and after bioink extrusion, as well as the rheological response of different bioinks to stress variations for efficient gel formation, a comprehensive assessment of the thixotropic properties of the bioink was conducted. As shown in Fig. 2Ab, after subjecting the bioinks to alternating low and high stress applications for three or four cycles, no significant changes were observed in the modulus compared to their initial value. Furthermore, all of the loss modulus exhibited a stable behavior. These findings provide evidence that different concentrations of PEO do not affect the nonlinear rheological characteristics of GelMA/PEO bioink systems within this stress range. The flow ramp mode was used to simulate the impact of shear force on ink behavior during the extrusion process. As the shear force increased, the viscosity of GelMA/PEO ink system with varying concentrations of PEO gradually decreased, exhibiting typical shear thinning characteristics. The overall viscosity of the ink system increased with higher PEO content. While the PEO concentration reaches 1 %, the overall viscosity did not significantly increase with further increases in PEO concentration (Fig. 2Ac).

The creep properties of GelMA/PEO inks formed with varying concentrations of PEO were investigated to evaluate the preservation of the directional microstructure induced by biphasic shear. As illustrated in Fig. 2Ad, upon repeated application of stress, the material undergoes instantaneous strain and exhibits a rapid exponential increase in compliance. This indicates that the material can promptly generate responsive strain under stress stimulation and achieve critical values within a short time, reflecting the immediate transmission and deformation process of bioink under extrusion pressure. During two cycles of stress treatment, the creep resistance of all the PEO containing materials weakened, meaning some residual creep not fully recovering. This phenomenon may contribute to maintaining the directional microstructure caused by shear stress during ink extrusion. Furthermore, an incremental decrease in creep resistance was observed as PEO concentration increased. Subsequently, the thixotropic behavior of different materials was further evaluated with the Flow peak hold mode. As illustrated in Fig. 2Ae, an increase of PEO concentration resulted in a corresponding elevation in viscosity. Importantly, higher concentrations of PEO weakened the viscosity recovery of different bioink during repeated stress application. However, once the PEO concentration exceeded 1 %, no significant alteration was observed in the viscosity recovery rate of GelMA/PEO ink.

The porosity of shear-oriented bioink was subsequently compared before and after PEO dissolution, with varying concentrations of PEO. As shown in Fig. 2B, the higher concentration of PEO resulted in larger pores remaining after PEO dissolution, consequently leading to higher overall material porosity. The stability of the oriented microstructures formed by GelMA/PEO bioink with varying concentrations of PEO treated with directional shear stress was further evaluated by printing scaffold structures in a Car support bath. In Fig. 2C, the microfilament structures printed by shear-oriented bioink exhibited apparent anisotropic properties in a Car support bath when the PEO concentration is equal to or greater than 1 %. Therefore, integrating the rheological results, PEO with a critical value of 1 % was used as an important component of the shear-oriented bioink in subsequent experiments. Finally, a scaffold structure with distinct anisotropic microstructure in both the inner and outer layers was fabricated in a Car support bath using the shear-oriented bioink ink containing 1 % PEO concentration through coaxial printing (Fig. 2D). The stability of this system for fabricating 3D oriented complex structures was validated.

In addition, the degradation efficiency of the GelMA/PEO hydrogel ink system was further evaluated under in vitro conditions through a degradation experiment using GelMA/PEO hydrogels containing 1 % 400w molecular weight PEO. As shown in Fig. S2, after soaking in sterile PBS for 14 days, the degradation efficiency of the GelMA/PEO ink was around 59 %. It is noteworthy that the GelMA/PEO hydrogel degraded very quickly after soaking at 37 °C for just 1 day, likely due to rapid mass reduction caused by PEO dissolution.

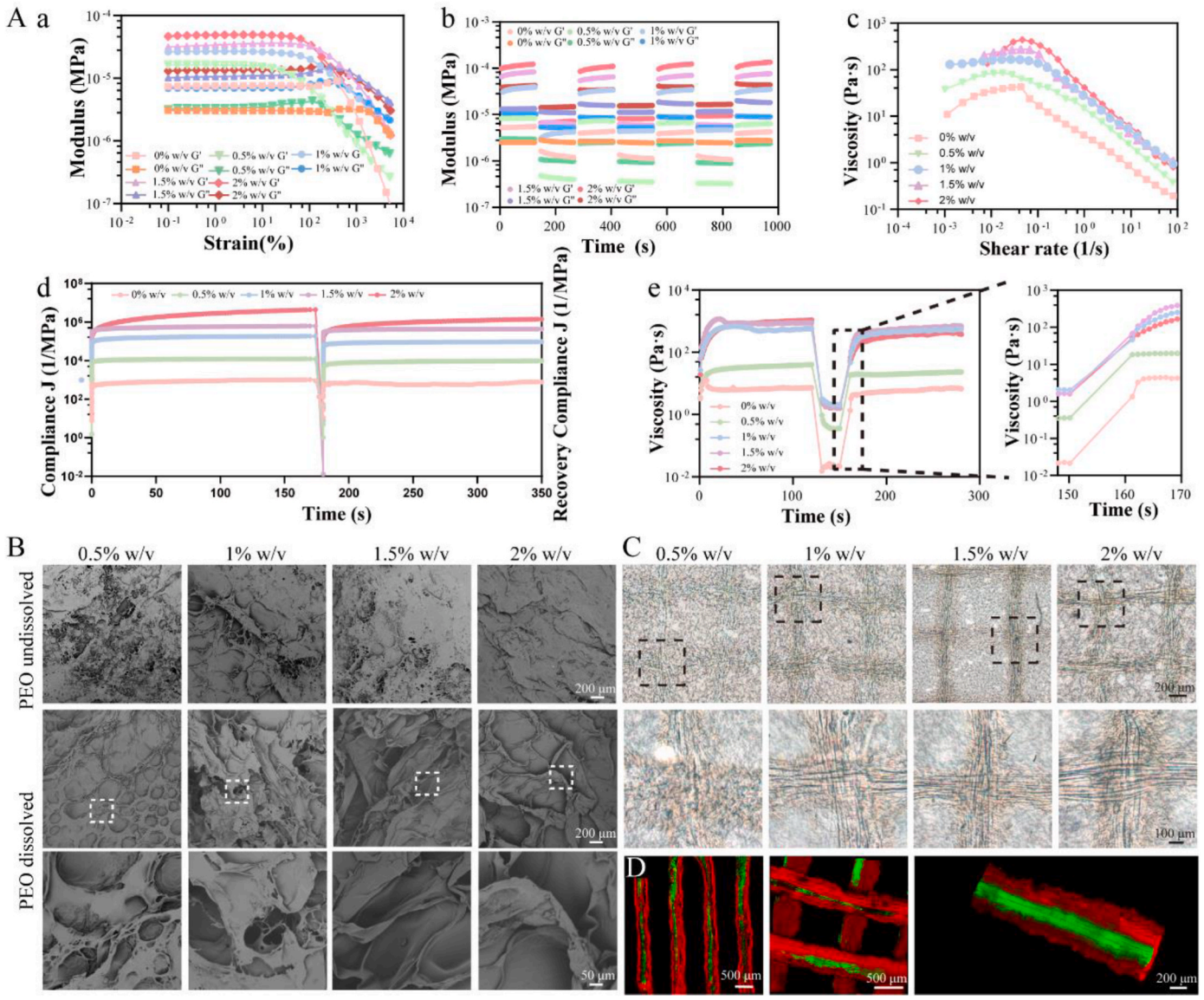

Fig. 2. The mechanical properties, porosity and directional orientation morphology of PEO/GelMA bioink with varying concentrations of 400w molecular weight PEO. (A) The influence effect of different PEO concentration to the rheology characteristics of PEO/GelMA hydrogel. (a) Storage modulus (G′) and loss modulus (G′′) curves. (b) Moduls-time curve under alternating high strain and low strain treating. (c) Viscosity-shear rate curve. (d) Creep-recovery compliance-time curve. (e) Viscosity recovery-time curve under alternating high strain and low strain. (B) Scanning electron microscopy (SEM) images of the different group GelMA/PEO hydrogel morphology before and after dissolving PEO. (C) The bright field images of scaffolds with anisotropic structure. (D) The optimal PEO concentration (1 %) used for coaxial printing stable oriented structures.

3.2. Printing parameters and properties

The shear-oriented bioink, containing 1 % PEO of 400w molecular weight and Rhodamine B labeled GelMA, was utilized in suspension printing to generate oriented microfibers within a 0.4 % κ-carrageenan support bath. The morphology and internal anisotropic microstructure of the printed fibers underwent analysis and characterization via confocal microscopy. As shown in Fig. 3A, with the needle maintaining a steady movement speed of 300 mm/min, a decrease in the extrusion rate of bioink corresponds to a reduction in the diameter of the produced microfibers. At an extrusion rate of 0.001 mL/min, the outcome is microfibers with diameters around 100 μm. With varying extrusion rates, the cross-section of the microfibers tends towards a circular shape, and there are visible signs of anisotropy within the structure of the fibers. These findings validated that the fiber diameter could be conveniently manipulated by altering the extrusion flow rate. By employing a fundamental volumetric equation, $\pi(d/2)^2 = Q/v$, where d represents the cross-sectional diameter of the microfiber, Q denotes the bioink's extrusion speed, and v signifies the speed of the nozzle, the circularity of oriented microfibers' cross sections printed at varying extrusion speeds was further quantitatively analyzed [30]. Fig. 3B demonstrated that the features have a cross-sectional aspect ratio close to 1 across all flow rates. These findings affirmed the viable application potential of this printing technique in harmoniously combining high resolution and anisotropic characteristics.

3.3. The fabrication of complex anisotropic structures

Traditionally, constructing concentric hierarchical structures with anisotropic traits often requires a complex process of concentrically rolling out directional lamellar structures [31,32]. With the anisotropic embedded 3D bioprinting system, it's possible to directly 3D printing concentric columnar structures in the stabilizing Car bath. As shown in Fig. 4A, the front and cross-sectional views exhibited exceptional

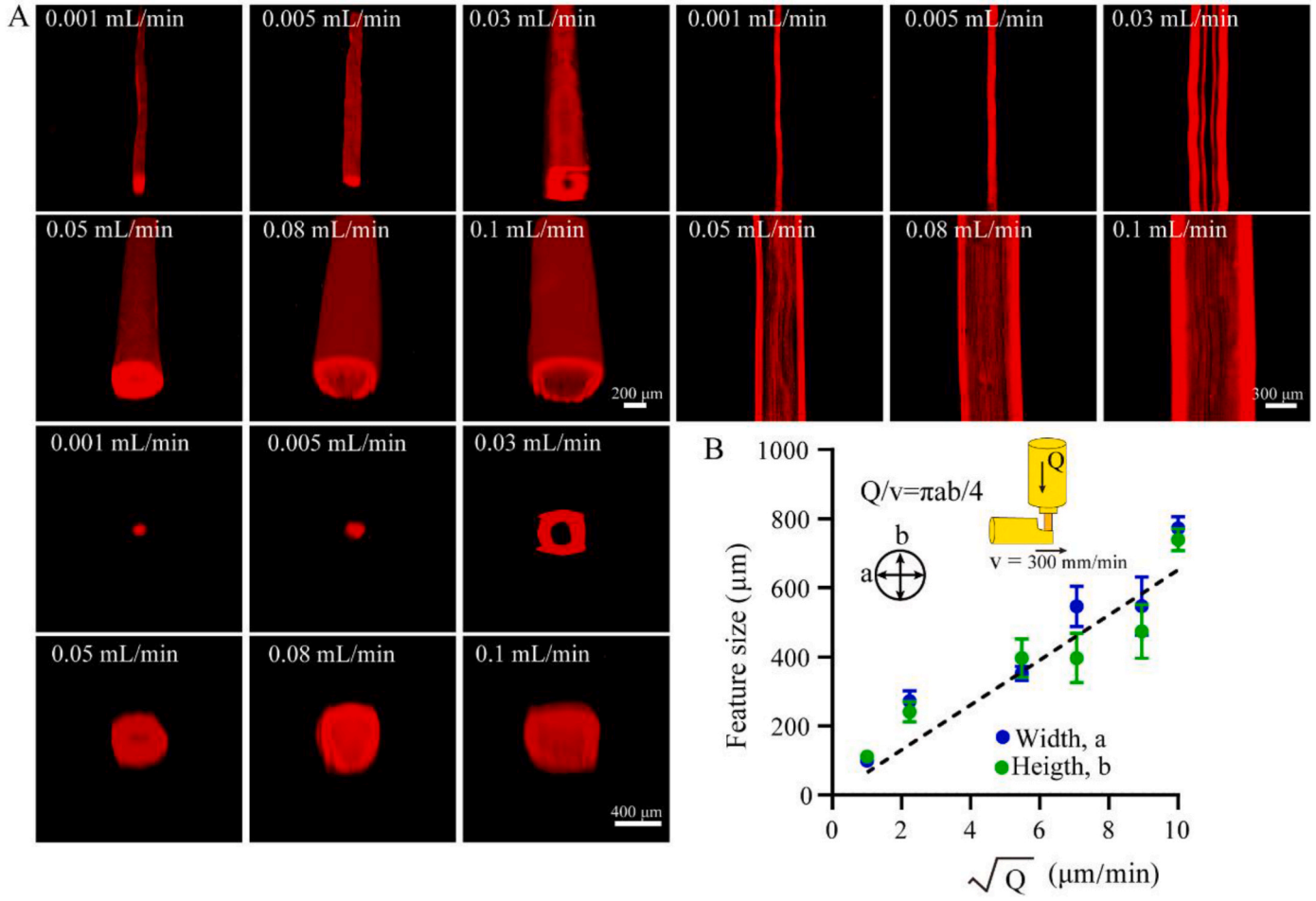

Fig. 3. The relationship between the printing speed and the thickness of the filament. (A) The confocal microscopy images of the thickness and morphology of the printed filaments. The roundness, cross section and oriented microstructure were all detected. Printing needle: inner diameter 0.26 mm, outer diameter 0.51 mm. (B) Feature size of printed objects can be controlled by the flow rate of the ink through the nozzle (Q), while the tangential velocity of the nozzle (v) was determined. The printed feature size shows nearly ideal behavior across a wide range of velocities and flow rates.

anisotropic microstructures. Additionally, the anisotropic printing system allowed for the direct creation of concentric hollow cylindrical surface, shown in 4B. These surfaces emerged from the layered configuration of anisotropic microwires, each measuring approximately 300 μm in diameter and thickness. Subsequently, by developing various curvature surfaces based on sine curves, it further confirmed the critical role of the printing path of the shear-oriented bioink in determining the directional orientation within the printed microfilaments (Fig. 4C&D).

Taking vascular tissue as an example, the shear-oriented bioink was printed in a Car supporting bath to create axial orientated artificial vascular tissue scaffolds with channel structures, as shown in Fig. 5. The vascular channel diameter was approximately 900 μm, the overall vascular diameter was about 2.5 mm, and the diameter of the GelMA/PEO microfilaments was roughly 100 μm. Inside the microfilaments, there were typical anisotropic characteristics. These results provided significant foundations for the application of shear-oriented bioink systems in the preparation of high-precision, orientated complex structures. Previous studies on the interaction between the matrix topography and cell orientation could be determined by the diameter of microfibers. When the microfibers with smaller diameters (almost 100 μm), cells tended to be aligned with microfibers [33,34]. Therefore, the microfibers fabricated by the GelMA/PEO suspension printing system not only possess anisotropic internal topological structures but also demonstrate unique advantages in promoting directional cell elongation due to their high precision, which is vital for the fabrication of artificial tissues with anisotropic characteristics.

3.4. Biological applications of the GelMA/PEO oriented printing system

While the shear-oriented bioink system exhibited tremendous application advantages in preparing anisotropic complex structures, further research was still needed on its orientational regulation of the cellular skeleton. As depicted in Fig. 6, the shear-oriented bioink was used to encapsulate different cells (C2C12, HUVEC, BMSCs, and MC-3T3) and print orientated scaffold structures. After 1 day of culure, the cells remained highly active with only a minimal number of dead cells observed. By the 3rd day, the cells began to stretch, and by the 7th day, most of the cells from all four groups were in a stretched state, with the skeleton of the cells aligning according to the direction of the scaffold. The quantitative analysis of the cell spreading directions for four different types of cells encapsulated within GelMA/PEO scaffolds after 7 days of culture were applied as the polar coordinate diagrams (Fig. S3). These data demonstrated that the oriented complex structures made by the shear-oriented bioink system hold potential for regulating the orientation of cytoskeleton. This establishes a solid foundation for the future creation of anisotropic artificial tissues.

Muscle tissue, which accounts for the highest content among the numerous anisotropic tissues in the human body, exhibits superior mechanical properties due to its axially oriented structural characteristics [35]. As shown in Fig. 7, a muscle patch measuring 2.5 mm × 2.5 mm × 1.2 mm was prepared. The oriented microfiber composed muscle patch was revealed by Rhodamine B-labeled GelMA, with a microfiber in approximately 200 μm diameter (Fig. 7A). C2C12 cells were

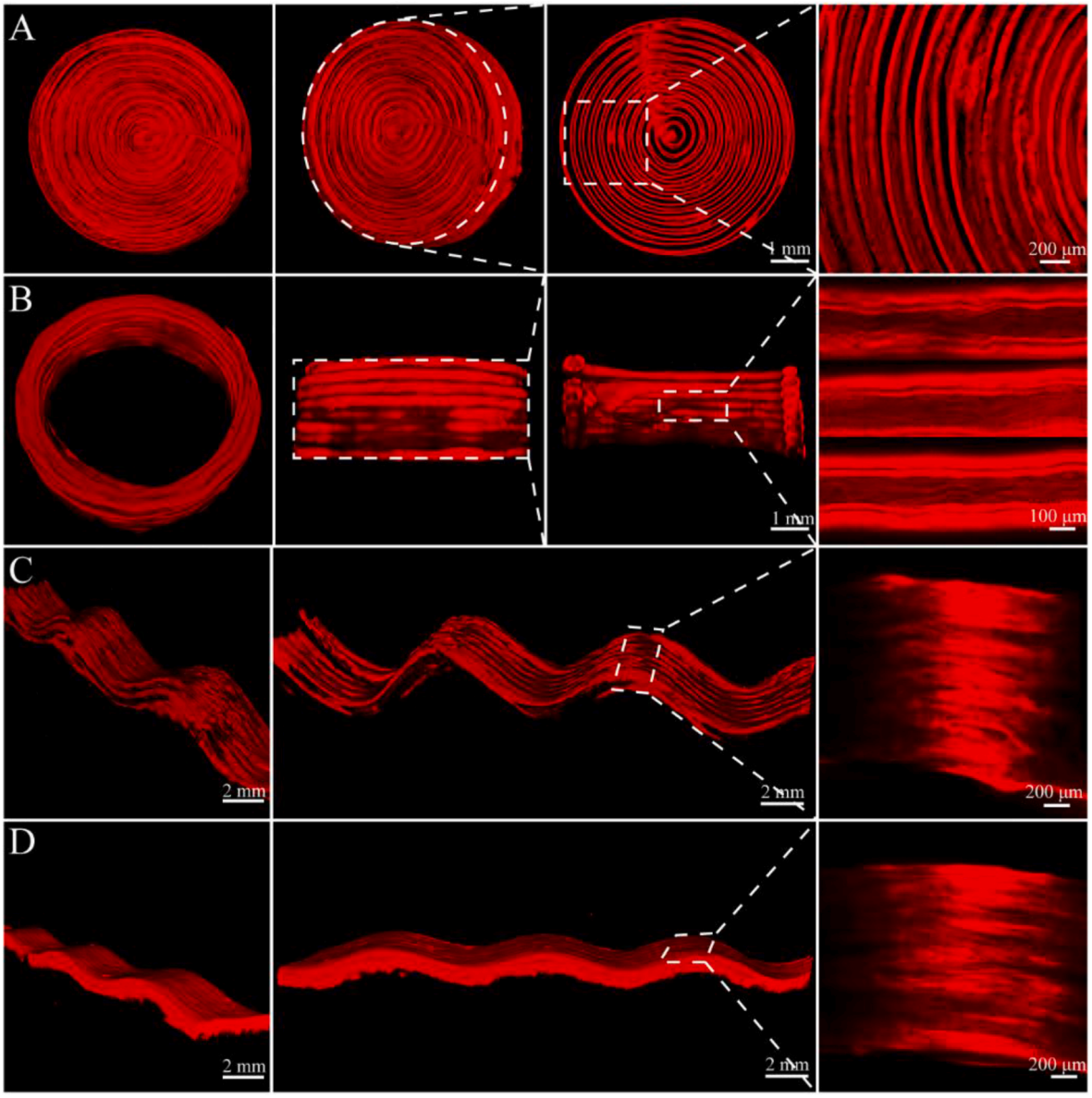

Fig. 4. The 3D structures composed of oriented microfilament, including columnar, tubular, and wave-like structures with varying curvatures. (A) The concentric hierarchical structures, (B) concentric hollow cylindrical surface, (C) and (D) surface with varying wave curvatures.

encapsulated in the shear-oriented bioink and used to bioprint the aforementioned patch structure. As shown in Fig. 7B, after seven days of in-vitro culture, almost all the interior cells of the muscle patch were stretched out, with the direction of most of the cell's skeletons growing along the filament direction of the patch structure. These results indicate that the shear-oriented bioink system holds great potential for preparing artificial tissues with anisotropic structural characteristics. Furthermore, compared to GelMA-based C2C12 cell-laden scaffolds, the anisotropic scaffolds printed with GelMA/PEO exhibited effective potential in promoting the directional spreading of C2C12 cells and the expression of Myosin and Myogenin proteins within the cells. Studies have shown that oriented topography can guide myotube alignment on various materials [36,37]. This explains how the oriented microstructures created by GelMA/PEO bioink enhance Myosin and Myogenin protein expression in C2C12 cells. These findings suggested that anisotropic microstructures prepared with GelMA/PEO materials can promote the maturation of C2C12 cells and enhance the expression of myotubes-related marker proteins to some extent and provided significant evidence for the in vitro fabrication of anisotropic artificial muscles based on the GelMA/PEO system.

In response to current research on anisotropic artificial tissue 3D bioprinting, such as bio-printing of microfiber-laden hydrogels [38,39], printing of anisotropic complex structures under magnetic stimulation [40], and 3D bioprinting of anisotropic tissues derived ECM hydrogel [41], the GelMA/PEO embedded 3D bioprinting system proposed in this study offers significant advantages, such as easy to operate, without additional stimulation, and outstanding printing precision, which are capable of producing highly accurate directional microfibers at the hundred microns level. This system holds great potential for personalized customization of biomimetic artificial anisotropic microtissues.

4. Conclusion

Repeating the directional characteristics of natural tissue in tissue engineering has already captured the interest of researchers in the field of functional tissue regeneration. This study has developed the anisotropic embedded 3D bioprinting system, opening a novel avenue for creating high-precision anisotropic structures. When considering the

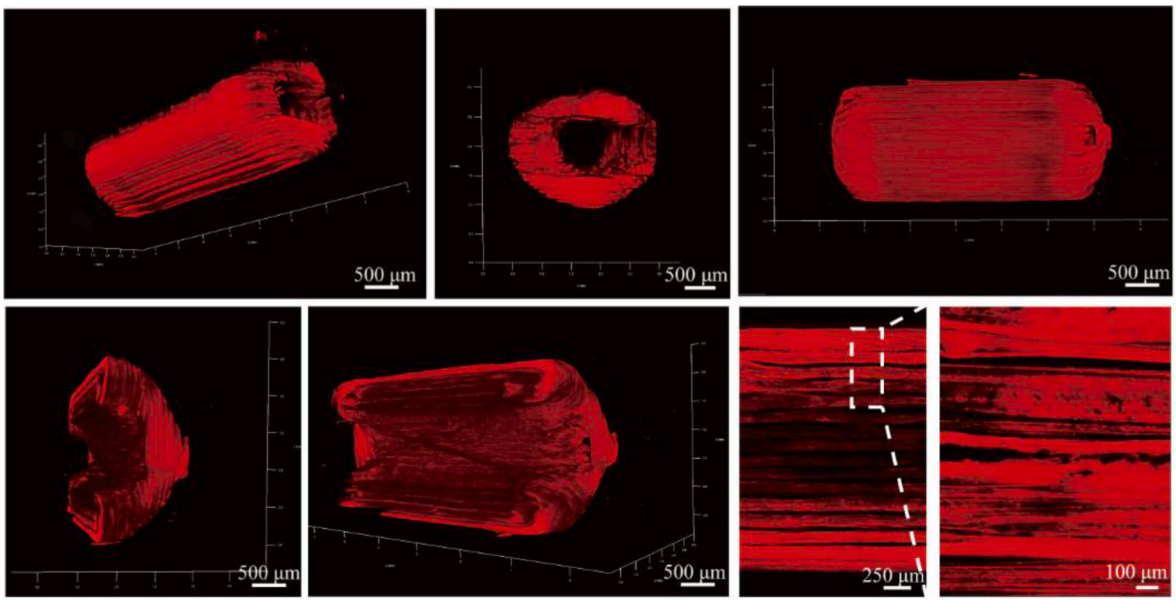

Fig. 5. Embedded printing the luminal structure with vascular flow channel and directional microstructures.

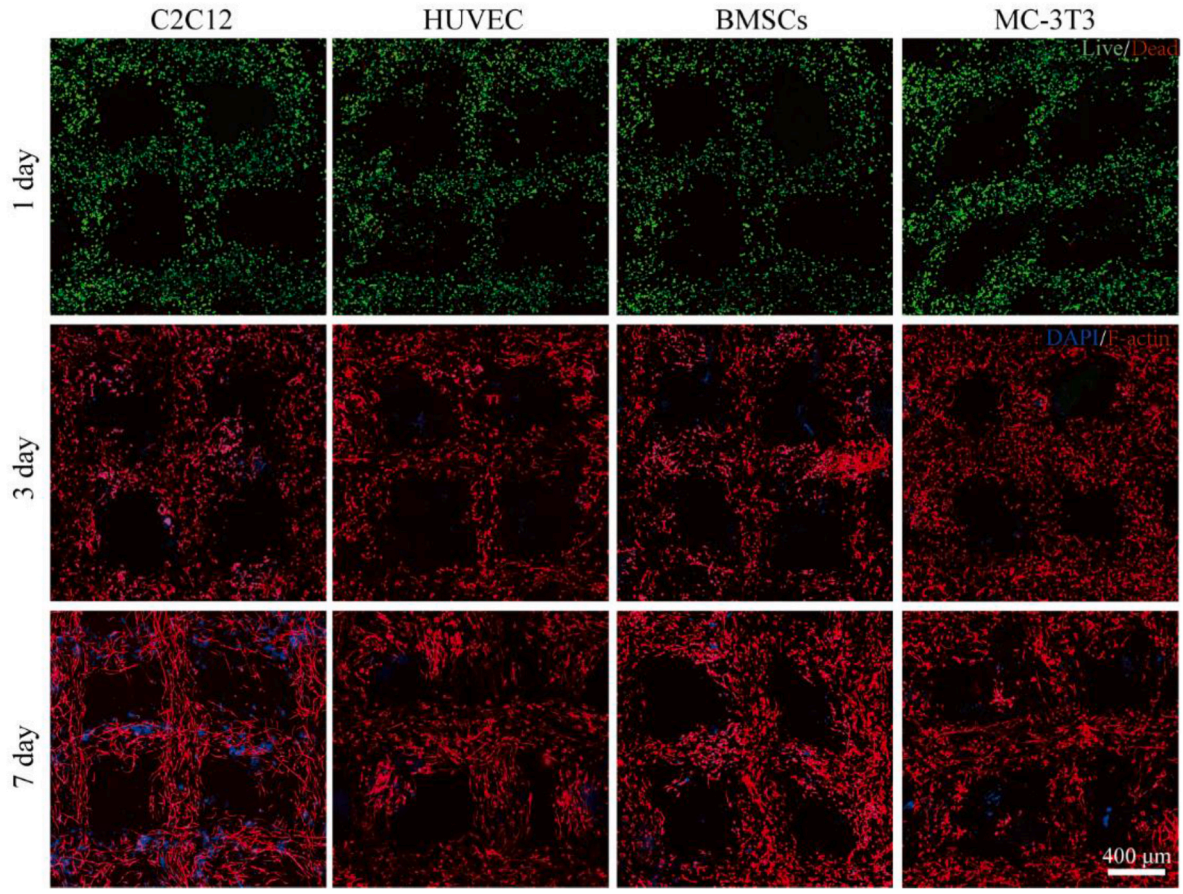

Fig. 6. The cellular viability and the cellular spreading. Fluorescence images of live/dead staining of C2C12, BMSCs, HUVECs and MC-3T3 encapsulated in oriented scaffold for 1 day. And the immunofluorescence images showing the morphologies of C2C12, BMSCs, HUVECs and MC-3T3 after 3 and 7 days of culture. Red: cytoskeleton. Blue: nucleus.

formation of directional microfibers post-extrusion of shear-oriented bioink system, which is temporarily sustained through the high viscosity of the ink itself and the encapsulation of the Car supporting bath, additional examination is warranted to enhance the ink system's stability for the fabrication of more intricate anisotropic bio-inspired structures. In general, the successful realization of this study offers fundamental possibilities for the efficient preparation and future clinical application of anisotropic biomimetic artificial tissues.

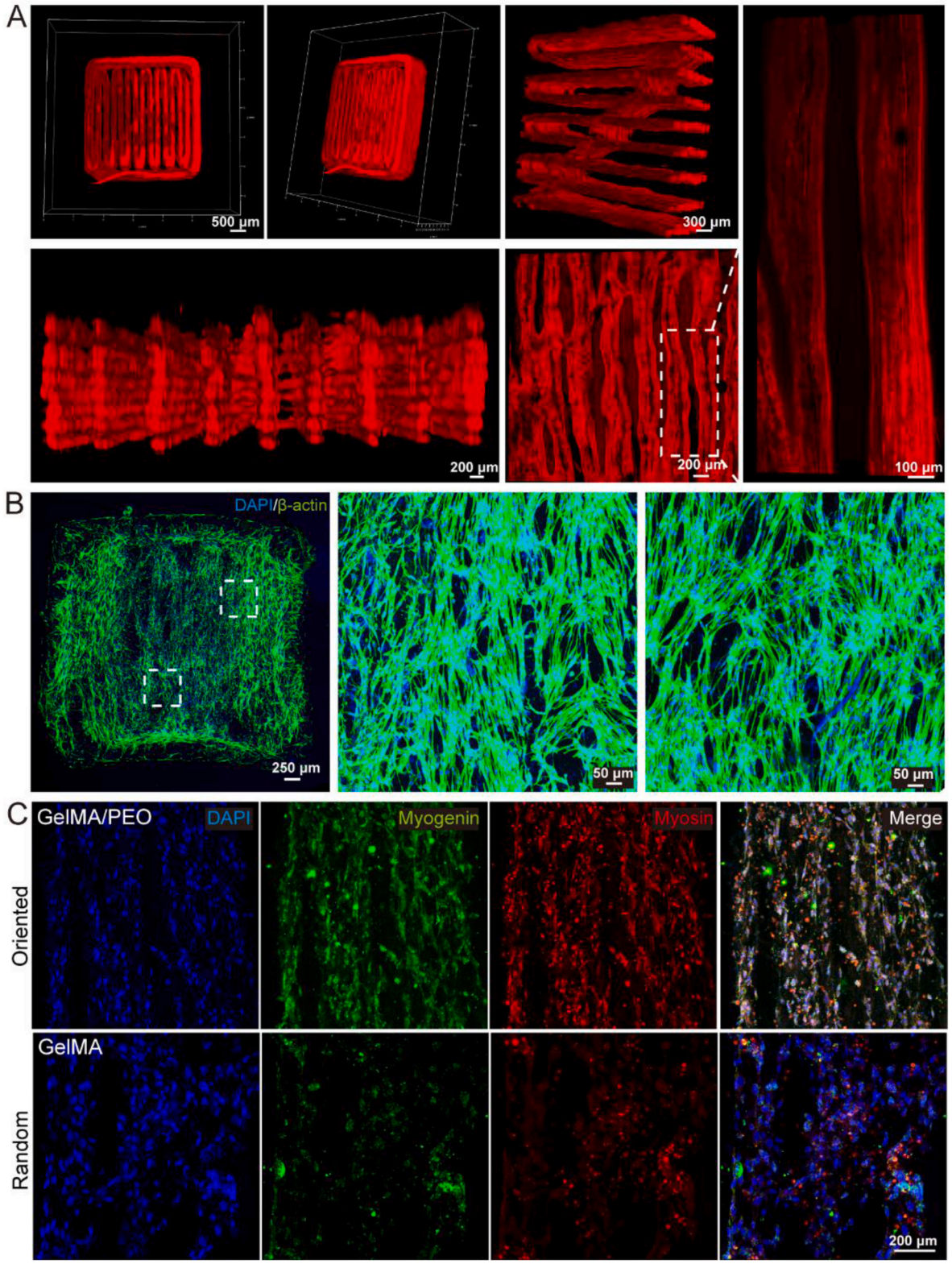

Fig. 7. Embedded printing the muscle patch. (A) PEO/Rhodamine B labeled GelMA bioink was used for printing the unidirectional arranged muscle patch structure. The microfilaments exhibit a well-defined and oriented microstructure internally. Red: Rhodamine B labeled GelMA. (B) C2C12 exhibited evident unidirectional elongation when loaded in the PEO/GelMA bioink and used to fabricate muscle patches. Green: cytoskeleton. Blue: nucleus. (C) Immunofluorescence staining results of Myogenin and Myosin proteins in C2C12 cells encapsulated in the GelMA and GelMA/PEO scaffolds after 7 days of culture.

Ethical approval

This article does not contain any studies with human or animal subjects performed by any of the authors.

CRediT authorship contribution statement

Lei Shao: Writing – review & editing, Writing – original draft, Supervision, Methodology, Investigation, Funding acquisition, Formal analysis, Data curation, Conceptualization. **Jinhong Jiang:** Methodology. **Chenhui Yuan:** Visualization. **Xinyu Zhang:** Visualization. **Lin Gu:** Visualization. **Xueping Wang:** Methodology, Investigation, Funding acquisition.

Declaration of competing interest

The authors declare that they have no known competing financial interests or personal relationships that could have appeared to influence the work reported in this paper.

Data availability

Data will be made available on request.

Acknowledgements

This work was financially supported by Natural Science Foundation of Zhejiang (LQ22C100001), Natural Science Foundation of Ningbo (2022J085), General scientific Research Project of Zhejiang Education Department (Y202044155), Open Foundation of the State Key Laboratory of Fluid Power and Mechatronic Systems (GZKF-202323), Natural Science Foundation of Zhejiang (LQ24C100001), Fundamental Research Funds for the Provincial Universities of Zhejiang (SJLY2024004).

Appendix A. Supplementary data

Supplementary data to this article can be found online at https://doi.org/10.1016/j.mtbio.2024.101160.

References

[1] J. Xing, N. Liu, N. Xu, W. Chen, D.J.A.F.M. Xing, Engineering complex anisotropic scaffolds beyond simply uniaxial alignment for tissue engineering, Adv. Funct. Mater. 32 (2022) 2110676, https://doi.org/10.1002/adfm.202110676.
[2] S. Harmansa, A. Erlich, C. Eloy, G. Zurlo, T. Lecuit, Growth anisotropy of the extracellular matrix shapes a developing organ, Nat. Commun. 14 (2023) 1220, https://doi.org/10.1038/s41467-023-36739-y.
[3] L. Shao, R. Hou, Y. Zhu, Y. Yao, Pre-shear bioprinting of highly oriented porous hydrogel microfibers to construct anisotropic tissues, Biomater. Sci. 9 (2021) 6763–6771, https://doi.org/10.1039/d1bm00695a.
[4] A. Abalymov, B.E. Pinchasik, R.A. Akasov, M. Lomova, B.V. Parakhonskiy, Strategies for anisotropic fibrillar hydrogels: design, cell alignment, and applications in tissue engineering, Biomacromolecules 24 (2023) 4532–4552, https://doi.org/10.1021/acs.biomac.3c00503.
[5] A. Pardo, M. Gomez-Florit, M.D. Davidson, M.O. Ozturk-Oncel, R.M.A. Domingues, J.A. Burdick, M.E. Gomes, Hierarchical design of tissue-mimetic fibrillar hydrogel scaffolds, Adv. Healthcare Mater. 24 (2024) e2303167, https://doi.org/10.1002/adhm.202303167.l.
[6] X. Lu, H. Jiao, Y. Shi, Y. Li, H. Zhang, Y. Fu, J. Guo, Q. Wang, X. Liu, M. Zhou, M. W. Ullah, J. Sun, J. Liu, Fabrication of bio-inspired anisotropic structures from biopolymers for biomedical applications: a review, Carbohydr. Polym. 308 (2023) 120669, https://doi.org/10.1016/j.carbpol.2023.120669.
[7] A. Velasco-Hogan, J. Xu, M.A. Meyers, Additive manufacturing as a method to design and optimize bioinspired structures, Adv Mater 30 (2018) e1800940, https://doi.org/10.1002/adma.201800940.
[8] Z. Wan, P. Zhang, Y. Liu, L. Lv, Y. Zhou, Four-dimensional bioprinting: current developments and applications in bone tissue engineering, Acta Biomater. 101 (2020) 26–42, https://doi.org/10.1016/j.actbio.2019.10.038.
[9] D.H. Kim, C.H. Seo, K. Han, K.W. Kwon, A. Levchenko, K.Y. Suh, Guided cell migration on microtextured substrates with variable local density and anisotropy, Adv. Funct. Mater. 19 (2009) 1579–1586, https://doi.org/10.1002/adfm.200990041.
[10] J. Wang, Q. Liu, J. Gong, Z. Wan, J. Zhou, C. Chang, D. Zhang, Micropatterned hydrogels with highly ordered cellulose nanocrystals for visually monitoring cardiomyocytes, Small 18 (2022) e2202235, https://doi.org/10.1002/smll.202202235.
[11] S. Liu, Z. Wang, X. Chen, M. Han, J. Xu, T. Li, L. Yu, M. Qin, M. Long, M. Li, H. Zhang, Y. Li, L. Wang, W. Huang, Y. Wu, Multiscale anisotropic scaffold integrating 3D printing and electrospinning techniques as a heart-on-a-chip platform for evaluating drug-induced cardiotoxicity, Adv. Healthcare Mater. 12 (2023) e2300719, https://doi.org/10.1002/adhm.202300719.
[12] B. Huang, E. Aslan, Z. Jiang, E. Daskalakis, M. Jiao, A. Aldalbahi, C. Vyas, P.J.A. M. Bártolo, Engineered dual-scale poly (ε-caprolactone) scaffolds using 3D printing and rotational electrospinning for bone tissue regeneration, Addit. Manuf. 36 (2020) 101452, https://doi.org/10.1016/j.addma.2020.101452.
[13] K. Deng, Z. Luo, L. Tan, Z. Quan, Self-assembly of anisotropic nanoparticles into functional superstructures, Chem. Soc. Rev. 16 (2020), https://doi.org/10.1039/d0cs00541j.
[14] Z. Zhang, M.L. Jorgensen, Z. Wang, J. Amagat, Y. Wang, Q. Li, M. Dong, M. Chen, 3D anisotropic photocatalytic architectures as bioactive nerve guidance conduits for peripheral neural regeneration, Biomaterials 253 (2020) 120108, https://doi.org/10.1016/j.biomaterials.2020.120108.
[15] M.T.I. Mredha, I. Jeon, Biomimetic anisotropic hydrogels: advanced fabrication strategies, extraordinary functionalities, and broad applications, J. P. i. M. S. Prog. Mater. Sci. 124 (2022) 100870 https://doi.org/10.1016/j.pmatsci.2021.100870.
[16] J. Chen, X. Liu, Y. Tian, W. Zhu, C. Yan, Y. Shi, L.B. Kong, H.J. Qi, K. Zhou, 3D-Printed anisotropic polymer materials for functional applications, Adv Mater 34 (2022) e2102877, https://doi.org/10.1002/adma.202102877.
[17] S.U. Khan, J.R. Pothnis, J. Kim, Manufacturing, Effects of carbon nanotube alignment on electrical and mechanical properties of epoxy nanocomposites, K. J. C. P. A. A. S. Compos Part A-Appl S 49 (2013) 26–34, https://doi.org/10.1016/j.compositesa.2013.01.015.
[18] M. Liu, Y. Ishida, Y. Ebina, T. Sasaki, T. Hikima, M. Takata, T.J.N. Aida, An anisotropic hydrogel with electrostatic repulsion between cofacially aligned nanosheets, Nature 517 (2015) 68–72, https://doi.org/10.1038/nature14060.
[19] M.T.I. Mredha, X. Zhang, T. Nonoyama, T. Nakajima, T. Kurokawa, Y. Takagi, J. P. Gong, Swim bladder collagen forms hydrogel with macroscopic superstructure by diffusion induced fast gelation, J. Mater. Chem. B 3 (2015) 7658–7666, https://doi.org/10.1039/c5tb00877h.
[20] M.T.I. Mredha, S.-G. Jeong, J.-K. Seon, I.J.S.M. Jeon, A diffusion-driven fabrication technique for anisotropic tubular hydrogels, Soft Matter 14 (2018) 7706–7713, https://doi.org/10.1039/c8sm01235k.
[21] E.J. Castanheira, L.P. Monteiro, V.M. Gaspar, T.R. Correia, J.M. Rodrigues, J. Mano, In-bath 3D printing of anisotropic shape-memory cryogels functionalized with bone-bioactive nanoparticles, F. J. A. A. M. ACS Appl. Mater. Interfaces 16 (2024) https://doi.org/10.1021/acsami.3c18290.
[22] G. Ying, N. Jiang, C. Yu, Y.S.J.B.-D. Zhang, Three-dimensional bioprinting of gelatin methacryloyl (GelMA), Bio Des Manuf 1 (2018) 215–224, https://doi.org/10.1007/s42242-018-0028-8.
[23] A. Guo, S. Zhang, R. Yang, C.J.M.T.B. Sui, Enhancing the mechanical strength of 3D printed GelMA for soft tissue engineering applications, Mater Today Bio 24 (2023) 100939, https://doi.org/10.1016/j.mtbio.2023.100939.
[24] K. Yue, G. Trujillo-de Santiago, M.M. Alvarez, A. Tamayol, N. Annabi, A. Khademhosseini, Synthesis, properties, and biomedical applications of gelatin methacryloyl (GelMA) hydrogels, Biomaterials 73 (2015) 254–271, https://doi.org/10.1016/j.biomaterials.2015.08.045.
[25] T.A. Lima, A. Fridman, J. McLaughlin, C. Francis, A. Clay, G. Narayanan, H. Yoon, M. Idrees, G.R. Palmese, J.L.J.I. Scala, E. Technologies, High-performance thermosets for additive manufacturing, Innovation and Emerging Technologies 10 (2023) 2330003, https://doi.org/10.1142/S2737599423300039.
[26] R. Zeinali, L.J. Del Valle, J. Torras, J. Puiggali, Recent progress on biodegradable tissue engineering scaffolds prepared by thermally-induced phase separation (Tips), J. I. j. o. m. s. Int. J. Mol. Sci. 22 (2021) 3504, https://doi.org/10.3390/ijms22073504.
[27] H. Budharaju, D. Sundaramurthi, S.J.B.M. Sethuraman, Embedded 3D bioprinting–an emerging strategy to fabricate biomimetic & large vascularized tissue constructs, Bioact. Mater. 32 (2024) 356–384, https://doi.org/10.1016/j.bioactmat.2023.10.012.
[28] K. Zhou, Y. Sun, J. Yang, H. Mao, Z. Gu, Hydrogels for 3D embedded bioprinting: a focused review on bioinks and support baths, J. J. o. M. C. B. J. Mater. Chem. B 10 (2022) 1897–1907, https://doi.org/10.1039/d1tb02554f.
[29] D.S. Wilkinson, W. Pompe, M. Oeschner, Modeling the mechanical behaviour of heterogeneous multi-phase materials, J. P. i. M. S. Prog. Mater. Sci. 46 (2001) 379–405, https://doi.org/10.3390/mi14071441.
[30] C.S. O'Bryan, T. Bhattacharjee, S. Hart, C.P. Kabb, K.D. Schulze, I. Chilakala, B. S. Sumerlin, W.G. Sawyer, T.E. Angelini, Self-assembled micro-organogels for 3D printing silicone structures, Sci. Adv. 3 (2017) e1602800, https://doi.org/10.1126/sciadv.1602800.
[31] D.S. Wilkinson, W. Pompe, M. Oeschner, Modeling the mechanical behaviour of heterogeneous multi-phase materials, J. P. i. M. S. Mater. Horiz. 46 (2001) 379–405, https://doi.org/10.1016/S0079-6425(00)00008-6.
[32] Y. Chen, C. Guo, E. Manousiouthakis, X. Wang, D.M. Cairns, T.T. Roh, C. Du, D. L. Kaplan, Bi-Layered tubular microfiber scaffolds as functional templates for engineering human intestinal smooth muscle tissue, Adv. Funct. Mater. 30 (2020), https://doi.org/10.1002/adfm.202000543.
[33] Y. Yang, X. Liu, D. Wei, M. Zhong, J. Sun, L. Guo, H. Fan, X. Zhang, Automated fabrication of hydrogel microfibers with tunable diameters for controlled cell

alignment, Biofabrication 9 (2017) 045009, https://doi.org/10.1088/1758-5090/aa90e4.
[34] Z. Qiu, H. Zhu, Y. Wang, A. Kasimu, D. Li, J.J.B.-D. He, Functionalized alginate-based bioinks for microscale electrohydrodynamic bioprinting of living tissue constructs with improved cellular spreading and alignment, Bio-Design and Manufacturing 6 (2023) 136–149, https://doi.org/10.1007/s42242-022-00225-z.
[35] S. Jana, S.K. Levengood, M. Zhang, Anisotropic materials for skeletal-muscle-tissue engineering, Adv Mater 28 (2016) 10588–10612, https://doi.org/10.1002/adma.201600240.
[36] M.T. Lam, S. Sim, X. Zhu, S.J.B. Takayama, The effect of continuous wavy micropatterns on silicone substrates on the alignment of skeletal muscle myoblasts and myotubes, Biomater 27 (2006) 4340–4347, https://doi.org/10.1016/j.biomaterials.2006.04.012.
[37] J.M. Dugan, R.F. Collins, J.E. Gough, S.J. Eichhorn, Oriented surfaces of adsorbed cellulose nanowhiskers promote skeletal muscle myogenesis, Acta Biomater. 9 (2013) 4707–4715, https://doi.org/10.1016/j.actbio.2012.08.050.
[38] M.E. Prendergast, M.D. Davidson, J.A.J.B. Burdick, A Biofabrication Method to Align Cells within Bioprinted Photocrosslinkable and Cell-Degradable Hydrogel Constructs via Embedded Fibers, vol. 13, 2021 044108, https://doi.org/10.1088/1758-5090/ac25cc.
[39] D.H. Kang, F. Louis, H. Liu, H. Shimoda, Y. Nishiyama, H. Nozawa, M. Kakitani, D. Takagi, D. Kasa, E. Nagamori, S. Irie, S. Kitano, M. Matsusaki, Engineered whole cut meat-like tissue by the assembly of cell fibers using tendon-gel integrated bioprinting, Nat. Commun. 12 (2021) 5059, https://doi.org/10.1038/s41467-021-25236-9.
[40] R. Tognato, A.R. Armiento, V. Bonfrate, R. Levato, J. Malda, M. Alini, D. Eglin, G. Giancane, T. Serra, A stimuli-responsive nanocomposite for 3D anisotropic cell-guidance and magnetic soft robotics, Adv. Funct. Mater. 29 (2018) 1804647, https://doi.org/10.1002/adfm.201804647.
[41] M.L. Terpstra, J. Li, A. Mensinga, M. de Ruijter, M.H.P. van Rijen, C. Androulidakis, C. Galiotis, I. Papantoniou, M. Matsusaki, J. Malda, R. Levato, Bioink with cartilage-derived extracellular matrix microfibers enables spatial control of vascular capillary formation in bioprinted constructs, Biofabrication 14 (2022), https://doi.org/10.1088/1758-5090/ac6282.